High-Throughput Preparation of New Photoactive Nanocomposites

High-Throughput Preparation of New Photoactive Nanocomposites

Eleonora Conterosito,[a] Iacopo Benesperi,[b] Valentina Toson,[a] Davide Saccone,[b] Nadia Barbero,[b] Luca Palin,[a, c] Claudia Barolo,[b] Valentina Gianotti,*[a] and Marco Milanesio*[a, d]

[a] *Dr. E. Conterosito, V. Toson, Dr. L. Palin, Dr. V. Gianotti, Dr. M. Milanesio Dipartimento di Scienze e Innovazione Tecnologica Università del Piemonte Orientale*
Viale Teresa Michel 11, 15121 Alessandria (Italy)
E-mail: valentina.gianotti@uniupo.it marco.milanesio@uniupo.it

[b] *I. Benesperi,[+] D. Saccone, Dr. N. Barbero, Prof. C. Barolo Dipartimento di Chimica and NIS and INSTM Reference Centre Università degli Studi di Torino*
Via P. Giuria 7, 10125 Torino (Italy)

[c] *Dr. L. Palin Nova Res s.r.l.*
Via Dolores Bello 3, 28100 Novara (Italy)

[d] *Dr. M. Milanesio*
CrisDi Interdepartmental Center for Crystallography

[+] *Present address: School of Chemistry Monash University*
Victoria 3800 (Australia)

Abstract

New low-cost photoactive hybrid materials based on organic luminescent molecules inserted into hydrotalcite (layered double hydroxides; LDH) were produced, which exploit the high-throughput liquid-assisted grinding (LAG) method. These materials are conceived for applications in dye-sensitized solar cells (DSSCs) as a co-absorbers and in silicon photovoltaic (PV) panels to improve their efficiency as they are able to emit where PV modules show the maximum efficiency. A molecule that shows a large Stokes' shift was designed, synthesized, and intercalated into LDH. Two dyes already used in DSSCs were also intercalated to produce two new nanocomposites. LDH in- tercalation allows the stability of organic dyes to be improved and their direct use in polymer melt blending. The prepared nanocomposites absorb sunlight from UV to visible and emit from blue to near-IR and thus can be exploited for light- energy management. Finally one nanocomposite was dis- persed by melt blending into a poly(methyl methacrylate)- block-poly(n-butyl acrylate) copolymer to obtain a photoactive film.

Introduction

Anionic clays are natural or synthetic layered mixed hydroxides with interlayer spaces that contain exchangeable anions.[1] Hy- drotalcite-like anionic clays, also known as layered double hy- droxides (LDHs), are the most representative examples of this family. LDHs are inorganic anionic layered solids of general formula $[M^{II}_{1-x}M^{III}_{x}(OH)_2]^{x+}(A^{n-})_{x/n}\bullet m\,H_2O$, the layer plane of which is constituted by bivalent and trivalent metals, usually in a M^{II}/M^{III} ratio of 2, coordinated octahedrally to six hydroxyl groups. The trivalent cations introduce a positive charge compensated by the presence of anions in the interlayer region.[1] Clay min- erals have attracted much interest thanks to their ability to intercalate a variety of ions, both inorganic and organic, which makes them useful materials in many fields, such as catalysis,[2] preparation of pigments,[3] removal of waste agents from water,[4–8] pharmaceutical and cosmetic formulations,[9–13] stabil- izers, photocatalytic materials for CO2 conversion,[14] rheology modifiers,[15] and luminescent compounds.[16] More specifically, hybrid organic–inorganic materials that involve the intercala- tion of dyes or photoactive compounds that include some out- standing materials, such as the Maya Blue[17] pigment, have been widely studied. Intercalation into LDH layers, besides sta- bilizing the organic molecules and protecting them from pho- tothermal degradation, is particularly useful in the case of pho- toactive materials, as it reduces intermolecular quenching and allows the tuning of their photoluminescence properties by modifying the interlayer environment through the modulation of the loading or the co-intercalation of surfactants.[18] Given the high density of positive charges in LDHs, the inorganic part contributes to the arrangement and structural orientation of the guest species. Moreover, the photoactive compound after the intercalation can be directly used in polymer melt blending.[19]

With particular regard to the photovoltaic (PV) field, photo- active materials can be exploited either directly, as solar light harvesters in dye-sensitized solar cells (DSSC)[20] and in poly- meric or small molecule organic photovoltaic (OPV) devices,[21] or indirectly, to obtain so-called “light management”.[22]
One of the main limitations to the efficiency of a PV cell is its inability to harvest all the wavelengths of the solar spec- trum with equal efficiency. In fact, rather different conversion efficiencies are observed at different wavelengths. Si-based solar cells, for instance, show the highest light conversion effi ciency at ð 600 nm that decreases to zero toward the near-IR (l ð 1100 nm) and UV regions (l ð 350 nm).[23] High-energy UV photons that are not converted may also cause degradation from the heating of the whole module and radical formation in the polymer envelope of the PV device. To overcome both problems a down-shifting technique can be applied by exploit- ing luminescent molecules that are able to tune the band- width of the light that reaches the PV cell. These molecules are able to shift higher-energy photons to wavelengths at which the absorption efficiency of the cell reaches its maximum.[24] Light management can be applied even more efficiently to DSSCs because of the sharper absorption of the organic dyes.[25, 26] Complementary dyes can be used in DSSCs to improve effi- ciency, the first one bound to titania, and the second one dis- persed in the electrolyte to act as a complementary pigment (energy relay dyes),[27] which mimics the photosynthetic pro- cess. The dispersion of DSSC dyes in LDHs allows their facile use in the melt blending extrusion of polymers.
The aim of this study is to develop low-cost, stable, and effi- cient materials based on photoactive molecules inserted into hydrotalcite that show significant capability for energy relay or down-shifting effects.
In previous studies, a liquid-assisted grinding (LAG) method was developed for the fast and clean preparation of organic- intercalated LDH nanocomposites.[28, 29] This method was used to demonstrate that the exchange of an inorganic anion (chlo- ride or nitrate) inside the LDH with an organic molecule that bears at least an acidic group is possible and easy to perform in an almost solvent-free environment. Very recently, efforts have been made to understand the potential and limitations of the LAG method and to optimize the intercalation yields on already known LDH-based compounds.[30] LAG is now a mature method, ready to be applied for the high-throughput produc- tion of new nanocomposites. In this study, we exploited the in- tercalation of photoactive molecules into LDH for both tradi- tional and innovative PV applications.
All the selected dyes (Figure 1) are already known for their optical properties (see the Experimental Section for details): B, D5, and VG1 are DSSC photosensitizers, and A and C present a large Stokes’ shift combined with interesting quantum yields (QY). Moreover, a carboxylic group is present in each molecule to enable the intercalation in the LDH structure, proposed here for the first time. After a laboratory scale intercalation of each molecule in LDH, we then concentrated our attention on the scale-up of the preparation of the best-performing synthe- sized molecule, dye A, for down-shifting technological applica- tions. This molecule, based on the dansyl moiety, shows the desired absorption and emission spectra and offers a good Stokes’ shift for the studied application, with a QY of at least 20 %, acceptable for technological applications.[31, 32]
The efficacy of the intercalation process and the reaction yield were evaluated by powder XRD, elemental analysis, and FTIR spectroscopy, and the effect of the intercalation on the thermal stability of the photoactive material was evaluated by thermogravimetric analysis (TGA). The host–guest interactions, which affect not only the distribution and orientation of the guests but also the photophysical and photochemical proper- ties of the material, were studied by evaluating the lumines- cence variations by liquid UV/Vis, UV/Vis diffuse reflectance, and fluorescence spectroscopy analyses in combination with the analysis of single-crystal and powder XRD data.
Finally, we produced a photoactive polymer able to absorb in the UV region and to emit in the cyan region of the optical spectrum at which silicon PV modules show a good conversion efficiency.

Results and Discussion

The preparation of new composite photoactive materials was carried out employing the LAG method developed by some of us.[28–30] The dyes tested for intercalation are shown in Figure 1 and are characterized by the presence of a carboxylic acid moiety to allow the bonding to LDH.
The LAG intercalation was first tested on photoactive com- pounds that were available in large (gram)

amounts thanks to their easy synthesis (B and D5). The method was then used on the double carboxylated squaraine dyes with different chain lengths (VG1-C2, VG1-C8, VG1-C10) and finally on two down- shifting compounds (dyes A and C). Of the seven tested dyes, A, B, and VG1-C2 gave promising yields of 66, 87, and > 80 % respectively, determined by powder XRD (Figures 2 and 3) as detailed in the Experimental Section. VG1-C10 was intercalated to achieve a yield of ð 7 %, and in the other three cases (C, D5, and VG1-C8) the yield was too low to be determined. Further- more, the dissolution of dyes demonstrated its key role in the intercalation process as discussed later. Single-crystal analysis is useful in the investigation of photoactive materials.[33–35] The single-crystal structures of A and B were solved to evaluate the interactions between the moieties and to infer a model for the packing of the dye inside the LDH layers and to unravel the information given by the d-spacing value. A more in-depth study of the partially successful and unsuccessful cases is needed to determine the reasons for the low yields.[36] The suc- cessful cases are discussed in more detail.

Dye B

The powder XRD pattern of dye B intercalated into LDH (LDH_ B), obtained by the LAG method, is reported in Figure 2, in which an arrow marks the basal peaks of the hybrid com- pound. The principal sign of intercalation is the presence of la- mellar peaks at a d-spacing higher than that of LDH_NO3 (8.80 Å). In the powder XRD pattern of LDH_B, the basal (0 0 1) peak of the LDH_B phase falls at Q = 0.288 Å-1, which corre- sponds to a d-spacing of 22.25 Å. The (0 0 3) peak of LDH_NO3 at Q = 0.715 Å-1, which corresponds to a d-spacing of 8.80 Å, and the peaks of crystalline B are small but still present (see Figure S8 for comparison), which indicates that the intercala- tion was not complete. The intercalated material, however, was formed in an appreciable amount, and the calculated yield is 87 %.

As the intercalation yield appears to be correlated to the sol- ubility of the guest molecule, the solubility of B was tested in different environments. The dye was more soluble in EtOH than in water. A higher pH favored the solubility of B in its anionic form. The color of the dye changed from orange (solid form or suspension in water) to yellow (dye in solution). There- fore, we tried the intercalation of B using different solutions (Table S3). From these experiments we obtained LDH_B sam- ples of different colors, which ranged from yellow to orange. As expected from the solubility tests in liquid, a yellow color of the sample indicates the deprotonation of the dye, which can be intercalated only in its anionic form, and therefore, corre- sponds to a higher intercalation yield, as observed from powder XRD data (Figure S10 and Table S3). Moreover, in the samples prepared without the use of NaOH, an intercalated phase with a shorter interlayer distance and was formed in low yield (Figure S10). The UV/Vis diffuse reflectance spectra of the samples were measured (Figure S11). However, it is difficult to estimate the intercalation yield from the UV/Vis spectra as dif- ferent effects influence their features. The correlation between the color of the sample and the intercalation yield can be seen in the results presented in Table S3.

The sample obtained with EtOH, which presented the best yield, was characterized by Raman spectroscopy and TGA. The Raman spectra of B alone, its sodium salt B_Na, and the inter- calated sample LDH_B are shown in Figures S12 and S13. In the Raman spectra the contribution of the LDH framework is negligible compared to the strong intensities of the bands owing to the more polarizable organic compound.[37, 38] This allows the determination of the effects of intercalation by direct comparison of the spectra of the intercalated molecule and the “free molecule”. Notably, in the low-wavenumber region (Figure S12), the evident decrease in the intensity of the ring breathing modes in the n˜ = 792–907 cm-1 region and of the C-C stretching modes, especially the C=C stretching band at n˜ = 1564 cm-1 in the spectrum of pure B compared to the spectra of the salt and the intercalated compound. This is determined by a more compact packing that hampers the vibra- tions of the molecules. Furthermore, the bands related to C-H in-plane deformation in aromatic rings that occur in the n˜ = 1283–1171 cm-1 region are weaker and less sharp in the spectra of the salt and especially the intercalated sample. The most intense peak in the spectrum of LDH_NO3 at n˜ = 1056 cm-1 is related to symmetric NO3 stretching. It is possible to see that the band at n˜ = 2215 cm-1 attributed to CN stretching in B is split in the spectra of the salt and of the intercalated compound because of the different environments (Figure S13).

To deepen the analysis from a structural viewpoint and get some insight on the possible packing of B moieties inside the layers, the crystal structure of B was solved by SC-XRD (Figure 4). The compound crystallizes in the P21/c monoclinic space group. The molecules are flat and interact to form dimers with

hydrogen bonds between the two carboxyl groups and p-stacking of the rings with a distance of 3.93 Å between the centers of the rings. The d-spacing of 22.25 Å minus the layer thickness corresponds to an interlayer space of 17.45 Å. As two molecules placed vertically in the dimer occupy ð 22.3 Å, we can infer that the molecules are slightly tilted inside the interlayer but are probably not interdigitated.
TGA profiles of LDH_B and B show the increased stability of the intercalated dye with respect to the free one (Figure S14). Compound B shows a two-step decomposition with a first weight loss of ð 20 % around 250 8C, which can be ascribed to the loss of CH3, CN, and COOH, and a second one centered at 300 8C that can be ascribed to the combustion of the aromatic ring. The intercalated sample shows a first weight loss below 200 8C, which is ascribed to the loss of interlayer water. The second weight loss centered at 235 8C is ascribed to the loss of surface adsorbed dye, and the intercalated dye is evolved in a single weight loss centered at 367 8C.

Squaraine dyes
The intercalation of squaraine dye VG1-C2 was obtained using the standard LAG method with a yield higher than 80 % (Figure 3). It is difficult to accurately estimate the yield of inter- calation as there is a superimposition of peaks of the interca- lated phase (marked by an arrow in Figure 3) of LDH_NO3 and of the possible LDH_CO_3 contaminant between 0.75 and 0.81 Å-1, which hampers a reliable fit of the powder XRD intensities. Different results among the VG series showed that longer alkyl chains lead to worse intercalation yields, which suggests that steric hindrance in the structure is a limitation for intercalation. The peculiarity of the intercalation of VG1-C2, beside the large dimensions of the molecule, is that there are two COOH groups on the same molecule and to intercalate the two groups must interact at the same time with both the top and the bottom layer. The d-spacing in LDH_VG1-C2, mea- sured by powder XRD, is 23.98 Å (which corresponds to an in- terlayer distance of 19.18 Å), and the molecule length was esti- mated for the isolated molecule (ð 22 Å hydrogen included) as it was not possible to grow single crystals. The powder XRD pattern of VG1-C2 (Figure 3) was resistant to any attempts of solution. Therefore, the VG1-C2 molecules could be slightly tilted to fit between the layers, given the interlayer distance.
TGA analysis of the sample is shown in Figure 5. The squaraine dye alone decomposes with four distinct weight losses.
The first weight loss, at ð 260 8C, can be associated with the loss of the aliphatic chains. Then, two distinct losses are visible between 300 and 400 8C, which are caused by the degradation of the skeleton of the molecule. Finally, carbonization occurs as indicated by the broad peak between 400 and 600 8C. Upon intercalation, the dye decomposes at higher temperatures, and two weight losses are attributed to the organic moieties : the first at 290 8C and the second between 450 and 520 °C.
IR spectra of LDH_VG1-C2 are shown in Figure S6.

Dye A
Dye A was chosen after a literature survey on fluorophore structures thanks to its interesting optical properties and easy synthesis[39] in view of a possible application in low-cost down- shifting polymers or as a co-absorber.[27] The simplest and cheapest way to obtain this dye is from the reaction between dansyl chloride and 6-aminohexanoic acid, through a nucleo- philic substitution between the chlorine and amine (Support- ing Information). The scale-up of the production of A from 1 to 10–20 g was straightforward, but the procedure led to a green glue instead of a solid. For this reason, a slightly modi- fied procedure for the purification of the sample was used (see Supporting Information), especially for the final drying process, and the characterization of the obtained product demonstrat- ed enough purity for our purpose. Dye A was then intercalated into LDH by the standard LAG procedure (see Experimental Section), and the product was characterized by powder XRD, TGA, and diffuse reflectance and emission spectroscopies. Fi- nally, the preparation of LDH_A was scaled up to 20 g, and LDH_A was used for the preparation of a photoactive polymer by melt blending.

Structural, thermal, and spectroscopic characterization
The powder XRD patterns of LDH_A, LDH_NO3, and A (Figure 2) indicate that, as a consequence of intercalation, the d-spacing increased from ð 8.80 Å in LDH_NO3 to 30.5 Å in LDH_A, as demonstrated by the presence of the (0 0 1) peak at Q = 0.206 Å-1 (d-spacing 30.5 Å). The (0 0 3) peak of LDH_NO3 is still

present, which indicates that the intercalation was not complete. The yield of intercalation, calculated as already de- scribed, is 66 %. The single-crystal structure of A was solved to evaluate the interactions between the moieties and infer a model for the packing of the dye inside the LDH layers to unravel the information given by the d-spacing value. Com- pound A crystallizes in the $P1^{-}$ space group, and the molecules (ð 17 Å long) are arranged in pairs connected by two hydro- gen bonds between the carboxyl groups (Figure 6). The pack- ing of A is also characterized by a hydrogen bond between the SO2 group and the hydrogen atom of the NH group and an interaction between the aromatic rings and the methyl group that points toward them (3.620 Å). The calculated dis- tance between one end of the molecule and the carboxylic oxygen atom of a facing molecule is 18.7 Å, which should be approximately the same length of the molecule plus its dis- tance from the layer when inside the LDH. The length of two molecules that are stacked with COOH groups pointing in op- posite directions is 25.593 Å (Figure 6). The d-spacing mea- sured by powder XRD in the LDH_A sample is ð 30 Å, which corresponds to an interlayer distance of ð 25 Å, in agreement with an arrangement of the molecules similar to that in the crystal of A. The samples prepared for down-shifting applica- tions were characterized by UV/Vis absorbance and fluores- cence spectroscopies. The diffuse reflectance spectra of LDH_A and A (Figure 7) are similar, therefore, the intercalation into LDH does not affect strongly the absorption features of the flu- orophore. Both spectra show a maximum absorption at l = 355 nm. In the spectrum of the intercalated sample LDH_A [Figure 7A (b)] , the band at l = 215 nm is caused by the elec- tronic transition of Mg-Al-LDH, the direct process from oxygen 2p to metal ns or np levels.[40] Moreover, the spectrum of LDH_ A shows a bathochromic shift and the broadening of the bands with respect to that of A [Figure 7A (a)]. The spectrum of LDH_A also shows a new band at l = 598 nm and a different absorption profile with respect to that of A. The difference in the relative intensity is owing to the dilution of A in the layered matrix, and the broad band centered at l = 625 nm is consistent with the slightly greenish color of the intercalated sample. The profile of the emission spectrum of LDH_A [Figure 7B (d)] , recorded upon excitation at l = 350 nm, exhibits an intense band that peaks at l = 500 nm. The band at l = 407 nm suggests the presence of aggregated molecules. The excitation spectrum of LDH_A [Figure 7B (c)] , recorded at l = 500 nm, shows two different absorptions centered at l = 365 and 420 nm. There is also an overlap between the emission and excitation bands typical of organic dyes, which contributes to re-absorption losses. From a comparison of the emission spectra of LDH_A, recorded in the solid state, and A, recorded in different solvents (Figure S3), the LDH environment was comparable to that of acetonitrile solvent. The Stokes' shift is equal to 150 nm, which is 88 nm less than that in water (Fig- ure S3 and Table S1 in the Supporting Information).
The TGA analysis of A shows a degradation that occurs in two steps demonstrated by two weight losses between 325 and 425 8C (Figure S14). The first step is the degradation of the aliphatic chain and the second is the degradation of the aro- matic rings. In the TGA of LDH_A a first loss below 200 8C be- cause of physisorbed water is visible. At higher temperatures, between 350 and 500 8C, two distinct weight losses are visible. The degradation of the organic part occurs at slightly higher temperatures with respect to that of the dye alone, together with the dehydroxylation of the layers and the loss of the re- sidual nitrate. Above 500 8C, the weight losses are owing to the carbonization of the sample. The FTIR spectrum of LDH_A is shown in Figure S7.

Scale-up of the nanocomposite production

Aiming towards the prototyping and implementation of a pho- toactive polymer for the encapsulation of PV modules, LDH_A was produced in larger amounts, as this sample is the most promising for the down-shifting application. The method opti- mized for the scale of 0.1 g of LDH gave low yields when applied to the intercalation of A into ð 20 g of LDH_NO3 in a single batch with manual grinding. This happened because the solubility of the dye, swelling of the LDH, and wettability of the physical mixture of dye and LDH become more relevant with larger amounts of reactants. Although we are aware that evaporation could be a problem, the comparison of the prod- uct obtained by grinding the same amount of LDH in the open manual mortar and in the closed electric ball-mill did not show remarkable differences, so we decided to employ the open mortar, which allowed the processing of larger batches. In the case of the intercalation of A in large batches, another approach was anyway necessary, as the main factor that affects the intercalation success was the dye solubility, which, in turn depends on the crystallinity of the synthesized dye. To shed light on the effect of the solvent on the intercalation yields, several LAG preparations with

solvents of different polarity were performed (Figure 8). Repeated intercalation was per- formed to improve the yield. Diethyl ether (Et2O), a nonpolar aprotic solvent, dichloromethane (CH2Cl2), a moderately polar aprotic solvent, and ethanol (EtOH), the polar protic solvent used in the standard synthesis, were tested. The aprotic sol- vent should be able to dissolve the dye in its neutral form and "push" the anionic form inside the layers. The calculated pKa of A is 3.28, as estimated by using a Marvin Calculator Plugin,[41] therefore, it should be already deprotonated in a sufficient amount using water as solvent. From preliminary tests, howev- er, the use of some NaOH was necessary. If we used CH2Cl2, an initial intercalation of 50% was achieved. The basal powder XRD peak is large and split (Figure S16 c), probably because of the co-intercalation of CH2Cl2. Anyway, if the sample is dried completely, the structure collapses and the yield decreases dra- matically (Figure S17) as seen for ibuprofen previously.[29] Given the lack of reproducibility, the use of CH2Cl2 was abandoned (Figure 8). Notably, repeating the intercalation on the same sample, without the addition of any dye but with the addition of only the solution and performing the grinding again (third and fourth columns of Figure 8) led to a significant increase of the yield, as it behaved as a kind of solid–liquid extraction (i.e. , from 50 to 75 % if Et2O was used and from 30 to 65 % if EtOH was used). From these tests we could conclude that, on a larger production scale, the best results in terms of yield of intercalation can be obtained using Et2O as solvent and repeat- ing the intercalation (Figure 8 and Figure S16). Finally, this method was adopted for the preparation of ð 20 g of interca- late. The amount was limited by the difficulty to hand-grinding a larger amount of compound thoroughly by using a large mortar. A large mechanical mill would be required to prepare larger batches of product. The powder XRD pattern of the ob- tained sample is shown in Figure S16 a.

Compounding of LDH_A-additivated polymer

A poly(methyl methacrylate)-block-poly(n-butyl acrylate) (PMMA-PnBA) block copolymer was employed for the com- pounding tests as it is characterized by high transparency and UV resistance. Preliminary tests of compounding were performed using different amounts of LDH_CO3 and LDH_NO3 in 5.0 g of polymer. The amount, 0.5 PHR (parts per hundred resin; i.e. , grams of additive per 100 g of polymer) of LDH in the polymer, was chosen after preliminary tests to maintain the high transparency of the film and adequate optical density. These tests allowed us to calibrate the compounder to find the best temperature, residence time, and velocity of the screws during circulation and extrusion. The temperature was set to 160 8C for the extrusion of PMMA/LDH_A, PMMA/LDH_CO3, and PMMA/LDH_NO3. The screw velocity and residence time were set as reported in Table S5. After the extrusion, the poly- mer strings were heat-pressed between two aluminum foils heated at 130 8C to obtain films of thicknesses between 190 and 290 mm (Figure 9). The dispersion of the LDH in the polymer was assessed by shining a UV lamp over the films (Figure 9) and by visual inspection by using an optical micro- scope (Figure S18). The dispersion of LDH_A appears to be good under UV light and by visual inspection under an optical microscope. No large aggregates can be seen. The processing in the laboratory compounder was not adequate to break the aggregates of LDH_NO3 and LDH_CO3, which had a diameter of ð 100–200 mm and were still visible in the film samples.

UV/Vis spectra were collected on the polymer films (Figure 10). The absorption of A centered at l = 336 nm is visi- ble, which proves that intercalation and compounding do not cause a significant shift in the absorption of the dye (see the UV/Vis spectra of A in different solvents in Figure S3). All spec- tra were scaled taking into account the effective thickness of the sample as an ideal thickness of 250 mm. Given the measured film absorption at l = 336 nm, the absorbance of 1.40 for a 250 mm thick film with 0.5 PHR of LDH_A can be estimat- ed. From this measurement it was possible to determine that the loading can be reduced to 0.35 PHR of LDH_A to maintain the desired optical density. A fluorescence emission spectrum was also recorded for the PMMA/LDH_A sample with excita- tion at l = 336 nm (Figure 10 b). The emission maximum is at l = 463 nm, close to the maximum efficiency region of silicon PV modules. The Stokes' shift is equal to l = 127 nm in this case, as the matrix effect shifts the emission toward the blue with respect to A in solution. This loading is the best compro- mise between absorbance in the down-shifting region and transparency. An amount of 100 g of compound would allow the preparation of 50 kg of photoactive polymer. As the typical thickness of the polymer film in a PV module is 250 mm, such an amount of photoactive polymer would lead to 212 m2 of photoactive polymer film.

The relationship between the optical properties and PV yield improvement is influenced by correlated parameters, as dis- cussed from an experimental and theoretical viewpoint by Alonso-Alvarez et al.[42] This model is based on the calculation of figures of merit, related to the absorption and emission properties, in relation to PV cell features, and allows the prediction of cell performance. If we consider the down-shifting properties of our photoactive film (high absorbance below l = 400 nm and transparency in the optical range, Stokes' shift of l = 127 nm, and QY of 40 %), an increase of the yield might be inferred. According to the parameters of Alonso-Alvarez et al., PMMA/LDH_A has an innovative approach with respect to the standard Lumogen family of compounds, which show a higher QY (50–100 %) but a much smaller Stokes's shift (l = 40– 50 nm). Of course, a deeper experimental and theoretical investigation is needed to assess the best technological path toward a successful application in real devices. The analysis of the fluorescence lifetime of PMMA/LDH_A showed the pres- ence of two populations. The first one, with a lifetime of 8.0 ns, represents 9% of the total and is comparable with the lifetime of dye A alone in solution (12.2 ns). The second one has a longer lifetime of 31.8 ns and represents 91 % of the total. Hence, the presence of these two populations can be as- cribed to the incomplete intercalation of A inside the LDH.

General LAG approach for the high-throughput production of nanomaterials

After the successful preparation of new nanomaterials, we can propose a detailed flowchart (Figure 11) that can be followed for the general application and optimization of the LAG method to the intercalation of new guest compounds, which exploits information obtained in the current and in previous studies.[29, 30] In detail, the procedure starts with a fast feasibility check using the standard recipe,[29] followed by the optimiza- tion of the recipe that exploits the Simplex chemometric method, which is able to explore efficiently, step-by-step, the space of chemical parameters that influence the reaction yield.[30] Finally, if the yield is too low, a second intercalation can be used to further improve it. This approach can be ex- tended to every material suitable for solid-state preparation.

Conclusions

The high-throughput screening of photoactive molecules inter- calated in layered double hydroxides (LDHs) was performed. Seven compounds (Figure 1) were tested, and three new hybrid nanocomposites were produced with yields above 60 %. Two nanocomposites, LDH_B and LDH_VG1-C2, represent the first successful intercalation of dyes designed for dye-sensitized solar cells into LDH. LDH_A is a new photoactive nanocompo- site with optical properties suitable for down-shifting applica- tions in silicon-based solar cells that is easily dispersible in photovoltaic polymers by melt blending. Therefore, in view of these technological applications and extended testing, the scale-up of the preparation of LDH_A was investigated to ex- ploit the mild, almost solvent-free, and facile liquid-assisted grinding (LAG) method. The new LDH_A nanocomposite was characterized from a physicochemical viewpoint by thermogra- vimetric analysis to assess its thermostability and by spectro- scopic methods to confirm that its photoactivity is suitable for down-shifting applications. Dye A absorbs at approximately l = 327 nm and emits at l = 490 nm, at which the PV light conversion efficiency of silicon is high. The solution of the single- crystal structure of A allowed us to infer that the deposition of A into the LDH layers is driven by the same forces as in the solid state (Figure 6). The p-stacking of the aromatic moieties and hydrogen bonds between hydroxyl and amino groups induce an interdigitated double layer (of ð 25 nm) that fits the experimental interlayer spacing of LDH_A perfectly if we con- sider the thickness of the layer and the hydrogen bond dis- tance between A and the layer.

The LAG method was adapted to the scale-up. When we in- crease the amounts of reactants, the system becomes more af- fected by dye solubility, which in turn depends on the crystal- linity of the synthesized dye, the swelling of the LDH, and the wettability of the physical mixture of the dye and LDH. The synthesis was scaled up successfully to prepare ð 20 g of prod- uct, and we obtained a yield of 75 % by manual grinding in a mortar. The resulting photoactive polymer can be employed directly to cover photovoltaic modules to improve their yields and stability.

The intercalation of the organic down-shifting dyes into hy- drotalcites by the optimized LAG approach (Figure 11) is un- precedented and it was exploited to improve dye stability and the ease of dispersion into polymers.[43] The proposed ap- proach to obtain an easy scale-up of the production of low- cost photoactive nanomaterials can be extended to many other classes of compounds and applications.

Experimental Section

The chemicals were purchased from Sigma–Aldrich or Alfa Aesar and used without further purification, except for carbonate hydrotalcite PURAL® MG 63 HT from SASOL, which was used after the substitution of the carbonate anion with nitrate following the pro- cedure described by Iyi et al.[44] The resulting material (LDH_NO3) has the formula [Mg0.68Al0.32(OH)2](NO3)0.32•0.37 H2O. The PMMA- PnBA block copolymer specifically designed for PV applications by Kuraray Co. (Japan) was chosen for the compounding tests be- cause of its high transparency and UV resistance.

Synthesis of dyes

Dyes were synthesized following procedures described by: Kong et al.[45] for dye A; Katz and Schilling[46] for dye B ; Barbero et al.[47, 48] for VG1-C2 and VG1-C8 ;[48] Etgar et al.[49] and Venditti et al.[50] for VG1-C10; and Gianotti et al.[51] for D5. Dye C was synthesized by the reaction of an amino intermediate prepared following the pro- cedure of Oliveira et al.[52] with succinic anhydride (see complete synthesis and characterization in the Supporting Information).

Preparation of intercalated compounds

The LAG method[28, 29] was adopted for the intercalation of anionic molecules into LDH and optimized for the larger scales of produc- tion. For these intercalations, a solution of 0.5 m NaOH in water and ethanol in a 2:1 ratio was prepared.[29] The guest molecule was first mixed and grinded in a mortar with LDH (0.1 g) in a 1:1 ratio with the exchange sites inside the LDH (i.e., the NO^{3-} ions), then 1 mL of the prepared solution was added with continuous grinding. The amount of liquid used for the intercalation was increased from the 0.5 mL of the preliminary tests to a final 1 mL for every0.1 g of LDH for solubility reasons. The dyes change their color upon intercalation, which depends on the pH of the system. After preparation, the samples were dried in an oven at 50 8C for 30 min or until complete dryness, which depended on the amount of product. These conditions are referred to as the “standard proce- dure”.

Characterization techniques

Relevant information on the characterization techniques is report- ed hereafter, and full details are available in the Supporting Infor- mation.

Characterization of dyes, intercalated compounds, and poly- mer films

The synthesized dyes were characterized by 1H (200 MHz) and 13C NMR spectroscopy (50 MHz) by using a Bruker Avance 200 NMR. ESI-MS experiments were conducted by using a Thermo Fin- nigan Advantage Max Ion trap spectrometer. UV/Vis spectra were recorded by using a Shimadzu UV-1700 spectrophotometer, and solid-state UV/Vis diffuse reflectance spectra were recorded by using a PerkinElmer Lambda 900. CHNS elemental analysis was per- formed by using a EuroVector CHN analyzer “EA3000”. TGA was performed by using a Setaram SETSYS Evolution instrument. FT- Raman spectra were measured by using a RFS-100 Bruker instru- ment. IR analyses were performed by using a FTIR Nicolet 5700 spectrometer (Thermo Optics). Optical properties were evaluated by using a DR UV-Vis (PerkinElmer Lambda 900) and by steady- state emission (Horiba Jobin–Yvon Model IBH FL-322 Fluorolog 2).

Diffraction techniques

Single-crystal diffraction data were collected by using an Oxford Xcalibur CCD area detector diffractometer. Structure solution was performed by using SIR2011,[53] and refinement with full-matrix least-squares was performed by using SHELXL-2013.[54] Marvin and Calculator Plugins[41] were used to draw chemical structures, prop- erty predictions, and calculations. powder XRD patterns were mea- sured by using a ThermoARL XTRA equipped with a solid-state Peltier-cooled detector and using CuKa radiation (l = 1.54062 Å).

The powder XRD patterns of the squaraine dyes and of LDH_VG1- C2, were measured at the European Synchrotron Radiation Facility (ESRF) in Grenoble because they were available in amounts too scarce (0.1 g) to be measured by using a laboratory diffractometer because of the cost and complexity of the synthesis. These meas- urements were performed at the SNBL BM01B Beamline using the standard Hi-Res powder

XRD setup and a wavelength of 0.50114 Å.[55, 56]

Intercalation yield calculations

In the powder XRD patterns of the intercalated samples the first peak (basal peak) is related directly to the interlayer spacing, thus the intercalation of large organic anions, compared to NO3 , leads to the appearance of basal peaks at lower angles. For this reason, the success of the intercalation reaction is indicated by the pres- ence of the (0 0 1), (0 0 2), and (0 0 3) reflections of the intercalated compounds at lower angles compared to those of the starting LDH_NO3 (Figures 2 and 3). The integrated intensities of the Bragg peaks in the powder XRD patterns were used to estimate the yield of intercalation. TOPAS Academic[57] software was used to perform a single-peak fit to measure the area of the residual (0 0 3) peak of LDH_NO3 and of the (0 0 1) peak of the intercalated compound LDH_GUEST. The percent yield was then calculated as follows [Eq. (1)]:

Yield % ¼ ½LDH GUEST=ðLDH GUESTþLDH NO3 Þ]* 100

The accuracy of the method to estimate the yields from powder XRD was verified by spectrophotometry. The sample was washed repeatedly with a known amount of solvent to remove the organic compound that did not enter the layers, then the solution was an- alyzed by using UV/Vis spectrophotometry, and the concentration was calculated using the Lambert–Beer law.[51] Knowledge of the amount of released organic compound with respect to the amount used to perform the intercalation allowed us to determine the yield of intercalation by difference (Figure S9). The yield deter- mined by using UV/Vis spectroscopy was similar to that estimated by using powder XRD, which confirms the reliability of the powder XRD refinements.

Compounding

Compounding tests were performed by using a laboratory Thermo HAAKE˘ MiniLab II Micro Compounder. The system is based on a conical, twin-screw compounder with an integrated backflow channel. As a result of the channel and a bypass valve, the resi- dence time can be finely controlled.
CCDC 1443531 (A) and 1443532 (B) contain the supplementary crystallographic data for this paper. These data can be obtained free of charge from The Cambridge Crystallographic Data Centre.

Acknowledgements

Piedmont Region FINPIEMONTE POR-FESR 2007/2013 project “Dye Hard” and FIRB 2012, “Multidisciplinary modeling of the structure of layered materials” (code RBFR10CWDA) are acknowledged for funding. Samuele Amede, Valeria Lagostina, and Giulio Barbaro are acknowledged for preparing the samples during their gradua- tion or master thesis. Dr. Marco Zanetti (University of Turin) is ac- knowledged for giving us access to the laboratory extruder. Ing. Roberto Faggino and INTECO s.r.l. are acknowledged for the col- laboration, compounding, and extrusion tests and for supplying the polymer. Prof. Davide Viterbo and Dr. Enrico Boccaleri are ac- knowledged for useful discussions during data analysis and manuscript preparation. Dr. Wouter Van Beek of SNBL beamline (ESRF Grenoble) is acknowledged for the synchrotron powder XRD patterns. Dr. Fabio Cucinotta is acknowledged for discus- sions regarding UV fluorescence spectroscopy.

Keywords: high-throughput screening • intercalations • layered compounds • photochemistry • polymers

References

[1] F. Trifirò, A. Vaccari in Solid State Supramol. Chem. (Eds.: G. Alberti, T. Bein), Pergamon Elsevier Science Ltd Press, Oxford 1996, pp. 1– 47.
[2] F. Figueras, Top. Catal. 2004, 29, 189 –196.
[3] U. Costantino, N. Coletti, M. Nocchetti, G. G. Aloisi, F. Elisei, Langmuir 1999, 15, 4454 –4460.
[4] D. Mohan, C. U. Pittman, J. Hazard. Mater. 2007, 142, 1 –53.
[5] V. Gianotti, M. Benzi, G. Croce, P. Frascarolo, F. Gosetti, E. Mazzucco, M. Bottaro, M. C. Gennaro,

Chemosphere 2008, 73, 1731 –1736.
[6] S. Angioi, S. Polati, M. Roz, C. Rinaudo, V. Gianotti, M. C. Gennaro, Envi- ron. Pollut. 2005, 134, 35– 43.
[7] S. Polati, S. Angioi, V. Gianotti, F. Gosetti, M. C. Gennaro, J. Environ. Sci.
Heal. Part B 2006, 41, 333 –344.
[8] S. Polati, F. Gosetti, V. Gianotti, M. C. Gennaro, J. Environ. Sci. Heal. Part B
2006, 41, 765 –779.
[9] C. Del Hoyo, Appl. Clay Sci. 2007, 36, 103 –121.
[10] M. I. Carretero, M. Pozo, Appl. Clay Sci. 2010, 47, 171 –181.
[11] H. Tamura, J. Ciba, M. Ito, T. Takeda, S. Kikkawa, Solid State Ionics 2004,
172, 607 –609.
[12] Z. P. (Gordon) Xu, G. Q. M. G. Q. (Max) Lu, Pure Appl. Chem. 2006, 78, 1771 –1779.
[13] A. Burzlaff, S. Brethauer, C. Kasper, B. O. Jackisch, T. Scheper, Cytometry Part A 2004, 62, 65– 69.
[14] J. L. Gunjakar, T. W. Kim, I. Y. Kim, J. M. Lee, S.-J. Hwang, Sci. Rep. 2013,
3, 2080.
[15] X. Yang, Q. Zhang, Polym. Int. 2004, 53, 698 –707.
[16] T. Posati, F. Bellezza, A. Cipiciani, F. Costantino, M. Nocchetti, L. Tarpani,
L. Latterini, Cryst. Growth Des. 2010, 10, 2847 –2850.
[17] M. Sfflnchez del RÞo, E. Boccaleri, M. Milanesio, G. Croce, W. van Beek, C. Tsiantos, G. D. Chyssikos, V. Gionis, G. H. Kacandes, M. Sufflrez, E. GarcÞa- Romero, J. Mater. Sci. 2009, 44, 5524 –5536.
[18] W. Shi, Z. Sun, M. Wei, D. G. Evans, X. Duan, J. Phys. Chem. C 2010, 114,
21070 –21076.
[19] Y. Gao, Y. Zhao, L. Qiu, Z. Guo, D. O'Hare, Q. Wang, Polym. Compos.
2015, DOI: 10.1002/pc.23764.
[20] J. Park, G. Viscardi, C. Barolo, N. Barbero, Chimia 2013, 67, 129 –135.
[21] G. Chen, H. Sasabe, T. Igarashi, Z. Hong, J. Kido, J. Mater. Chem. A 2015,
3, 14517– 14534.
[22] W. G. J. H. M. van Sark, Renewable Energy 2013, 49, 207 –210.
[23] W. Shockley, H. J. Queisser, J. Appl. Phys. 1961, 32, 510 –519.
[24] E. Klampaftis, D. Ross, K. R. McIntosh, B. S. Richards, Sol. Energy Mater.
Sol. Cells 2009, 93, 1182 – 1194.
[25] F. Bella, G. Griffini, M. Gerosa, S. Turri, R. Bongiovanni, J. Power Sources
2015, 283, 195 –203.
[26] G. Griffini, F. Bella, F. Nisic, C. Dragonetti, D. Roberto, M. Levi, R. Bongio- vanni, S. Turri, Adv. Energy Mater. 2015, 5, 1401312.
[27] G. Y. Margulis, B. Lim, B. E. Hardin, E. L. Unger, J.-H. Yum, J. M. Feckl, D. Fattakhova-Rohlfing, T. Bein, M. Gratzel, A. Sellinger, M. D. McGehee, Phys. Chem. Chem. Phys. 2013, 15, 11306 – 11312.
[28] M. Milanesio, E. Conterosito, D. Viterbo, L. Perioli, G. Croce, Cryst.
Growth Des. 2010, 10, 4710 –4712.
[29] E. Conterosito, L. Palin, G. Croce, L. Perioli, D. Viterbo, G. Gatti, M. Mila- nesio, W. Van Beek, Cryst. Growth Des. 2013, 13, 1162 – 1169.
[30] V. Toson, E. Conterosito, L. Palin, E. Boccaleri, M. Milanesio, V. Gianotti,
Cryst. Growth Des. 2015, 15, 5368 –5374.
[31] Y.-H. Li, L.-M. Chan, L. Tyer, R. T. Moody, C. M. Hirnel, D. M. Hercules, J. Am. Chem. Soc. 1975, 97,
3118– 3126.
[32] C. M. Himel, R. T. Mayer, Anal. Chem. 1970, 42, 130 –132.
[33] R. Gobetto, G. Caputo, C. Garino, S. Ghiani, C. Nervi, L. Salassa, E. Rosen- berg, J. B. A. Ross, G. Viscardi, G. Martra, I. Miletto, M. Milanesio, Eur. J. Inorg. Chem. 2006, 2839 –2849.
[34] A. Albertino, C. Garino, S. Ghiani, R. Gobetto, C. Nervi, L. Salassa, E. Rosenberg, A. Sharmin, G. Viscardi, R. Buscaino, G. Croce, M. Milanesio, J. Organomet. Chem. 2007, 692, 1377 –1391.
[35] M. Milanesio, D. Viterbo, A. Albini, E. Fasani, R. Bianchi, M. Barzaghi, J. Org. Chem. 2000, 65, 3416 –
3425.
[36] E. Conterosito, M. Milanesio, L. Palin, V. Gianotti, "Rationalization of LAG intercalation yields of organic molecules into Layered Double Hydrox- ides by multivariate analysis", unpublished results, 2016.

[37] E. Conterosito, G. Croce, L. Palin, C. Pagano, L. Perioli, D. Viterbo, E. Boc- caleri, G. Paul, M. Milanesio, Phys. Chem. Chem. Phys. 2013, 15, 13418 – 13433.
[38] A. Arrais, E. Diana, R. Gobetto, M. Milanesio, D. Viterbo, P. L. Stanghellini, Eur. J. Inorg. Chem. 2003, 1186 – 1192.
[39] Y. H. Li, L. M. Chan, L. Tyer, R. T. Moody, C. M. Hirnel, D. M. Hercules, J. Am. Chem. Soc. 1975, 97, 3118– 3126. .
[40] A. A. A. Ahmed, Z. A. Talib, M. Z. bin Hussein, A. Zakaria, J. Solid State Chem. 2012, 191, 271 –278.
[41] Chemaxon, 2015, (http://www.chemaxon.com).
[42] D. Alonso-Alvarez, D. Ross, E. Klampaftis, K. R. McIntosh, S. Jia, P. Storiz, T. Stolz, B. S. Richards, Prog. Photovoltaics 2015, 23, 479 –497.
[43] L. A. Utracki, M. Sepehr, E. Boccaleri, Polym. Adv. Technol. 2007, 18, 1 – 37.
[44] N. Iyi, H. Yamada, T. Sasaki, Appl. Clay Sci. 2011, 54, 132 –137.
[45] Y. Kong, M. Jung, K. Wang, S. Grindrod, A. Velena, S. A. Lee, S. Dakshana- murthy, Y. Yang, M. Miessau, C. Zheng, A. Dritschilo, M. L. Brown, Cancer Ther. 2011, 10, 1591 –1599.
[46] H. E. Katz, M. L. Schilling, J. Am. Chem. Soc. 1989, 111, 7554 –7557.
[47] N. Barbero, C. Magistris, J. Park, D. Saccone, P. Quagliotto, R. Buscaino, C. Medana, C. Barolo, G. Viscardi, Org. Lett. 2015, 17, 3306 –3309.
[48] J. Park, C. Barolo, F. Sauvage, N. Barbero, C. Benzi, P. Quagliotto, S. Co- luccia, D. Di Censo, M. Gratzel, M. K. Nazeeruddin, G. Viscardi, Chem. Commun. 2012, 48, 2782 –2784.
[49] L. Etgar, J. Park, C. Barolo, V. Lesnyak, S. K. Panda, P. Quagliotto, S. G. Hickey, M. K. M. K. Nazeeruddin, A. EychmUller, G. Viscardi, M. Gratzel, RSC Adv. 2012, 2, 2748 –2752.
[50] I. Venditti, N. Barbero, M. V. Russo, A. Di Carlo, F. Decker, I. Fratoddi, C. Barolo, D. Dini, Mater. Res. Express 2014, 1, DOI: 10.1088/2053 –1591/1/ 1/015040.
[51] V. Gianotti, G. Favaro, L. Bonandini, L. Palin, G. Croce, E. Boccaleri, E. Artuso, W. van Beek, C. Barolo, M. Milanesio, ChemSusChem 2014, 7, 3039 –3052.
[52] F. F. D. Oliveira, D. C. B. D. Santos, A. A. M. Lapis, J. R. CorrÞa, A. F. Gomes, F. C. Gozzo, P. F. Moreira, V. C. de Oliveira, F. H. Quina, B. A. D. Neto, Bioorg. Med. Chem. Lett. 2010, 20, 6001 –6007.
[53] M. C. Burla, R. Caliandro, M. Camalli, B. Carrozzini, G. L. Cascarano, C. Giacovazzo, M. Mallamo, A. Mazzone, G. Polidori, R. Spagna, J. Appl. Crystallogr. 2012, 45, 357 –361.
[54] G. M. Sheldrick, Acta Crystallogr. Sect. D 2010, 66, 479 –485.
[55] E. Boccaleri, F. Carniato, G. Croce, D. Viterbo, W. van Beek, H. Emerich, M. Milanesio, J. Appl. Crystallogr. 2007, 40, 684 –693.
[56] W. Van Beek, F. Carniato, S. Kumar, G. Croce, E. Boccaleri, M. Milanesio, Phase Transitions 2009, 82, 293 –302.
[57] A. A. Coelho, Topas-Academic. General Profile and Structure Analysis Soft- ware for Powder Diffraction Data, Version 5, 2012.

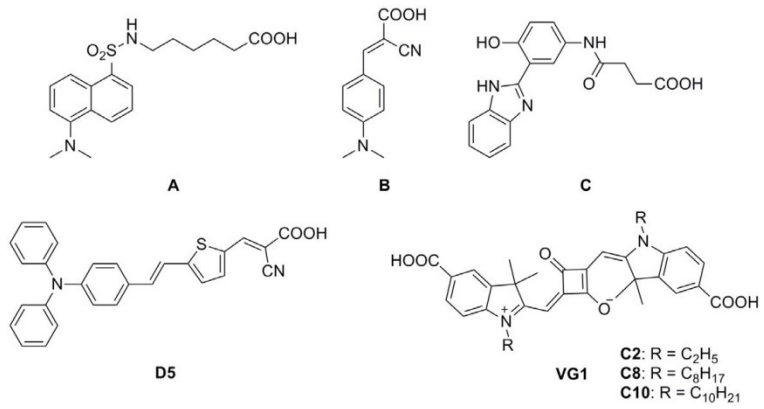

Figure 1. Molecular structures of the employed dyes.

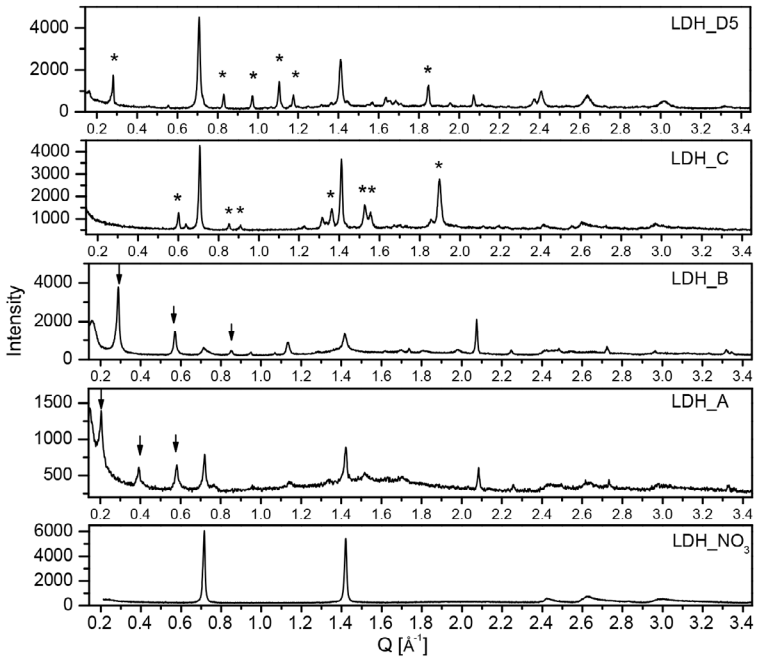

Figure 2. Powder XRD patterns of the intercalated dyes. The arrows mark the positions of the basal peaks of the intercalated phase, if present. The stars mark the position of the main peaks of the residual crystalline dye.

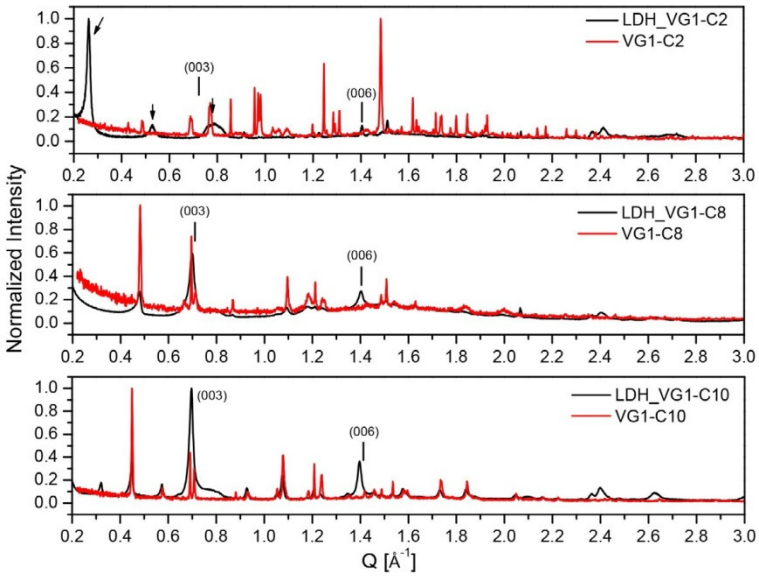

Figure 3. Powder XRD patterns of squaraine dyes A) VG1-C2, B) VG1-C8, and C) VG1-C10 intercalated in LDH_NO3 (black) and alone (red). The line marks the position of the (0 03) peak of LDH_NO3 that could be present as a residue.

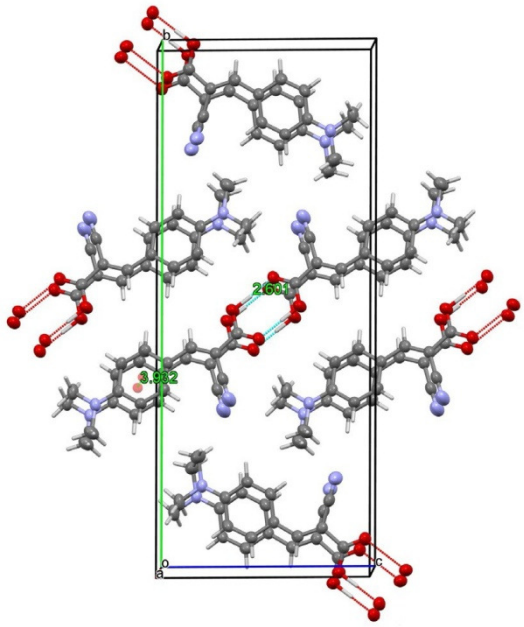

Figure 4. Crystal structure packing of B that shows the interactions between the molecules and related distances.

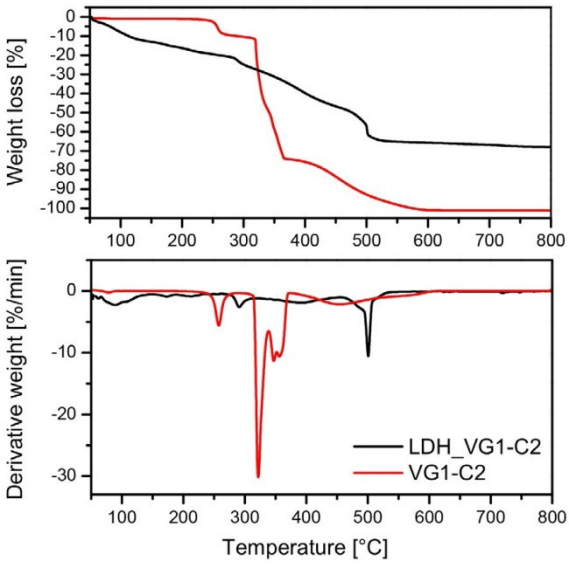

Figure 5. TGA analysis of VG1-C2 and LDH_VG1-C2.

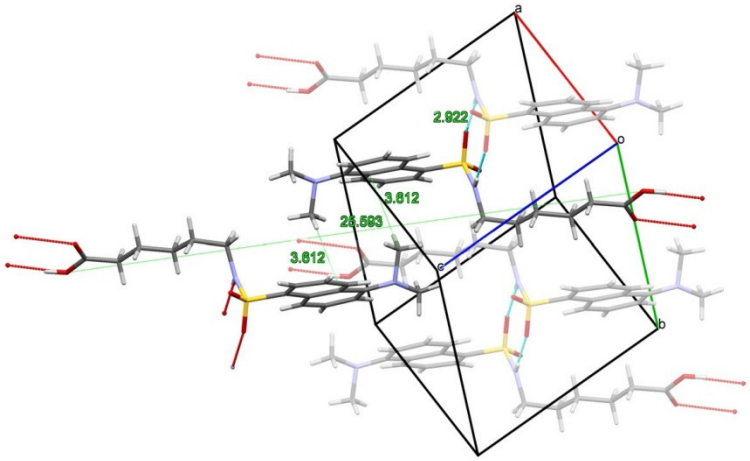

Figure 6. Detail of the crystal structure of A that shows the interactions between the molecules and related distances.

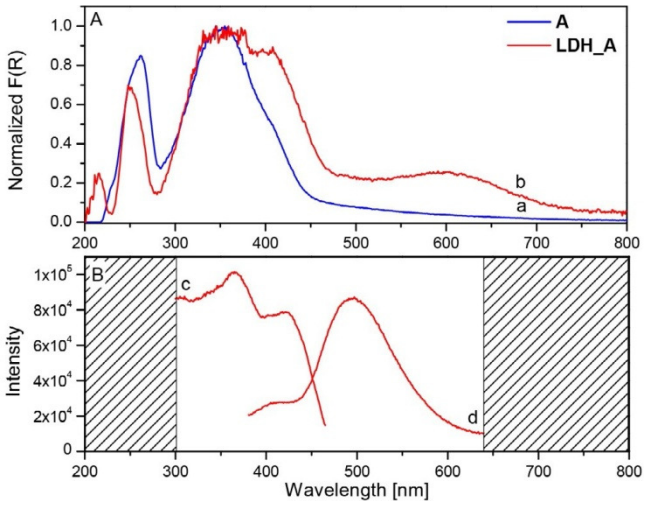

Figure 7. A) Diffuse reflectance spectra of a) A and b) LDH_A dispersed in BaSO4 and normalized to 1 in the inset; B) Overlap of c) excitation (at l = 500 nm) and d) emission (excited at l = 350 nm) spectra of LDH_ A after arbitrary scaling of the intensities to facilitate the comparison.

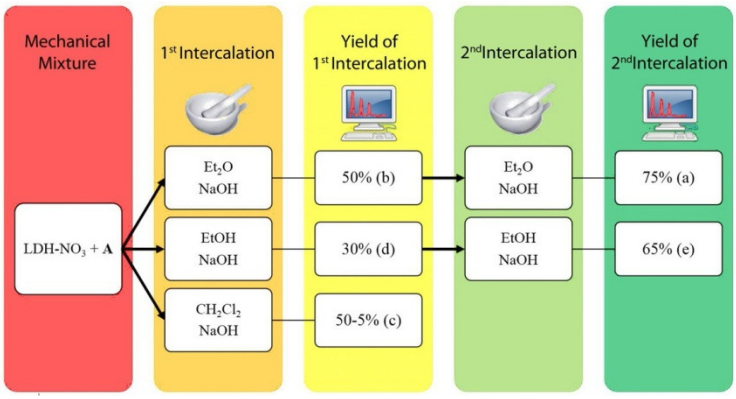

Figure 8. Summary of the tests with different solvents and repeated intercalation. The powder XRD patterns of the samples indicated by the letters in paren- thesis are shown in Figure S16.

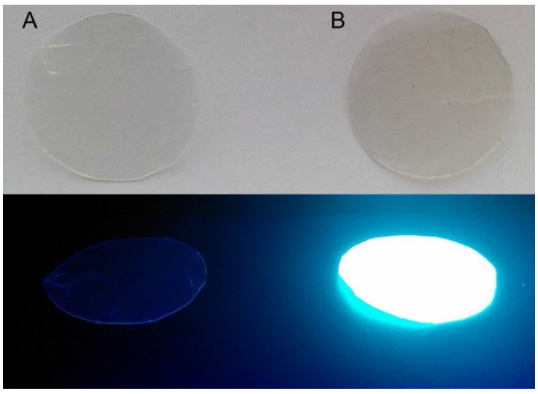

Figure 9. Pictures of the films obtained by pressing the polymer after extru- sion in the laboratory compounder under visible light (top) and UV light (bottom): A) polymer compounded with LDH_NO3 ; B) polymer compounded with 0.5 PHR of LDH_A.

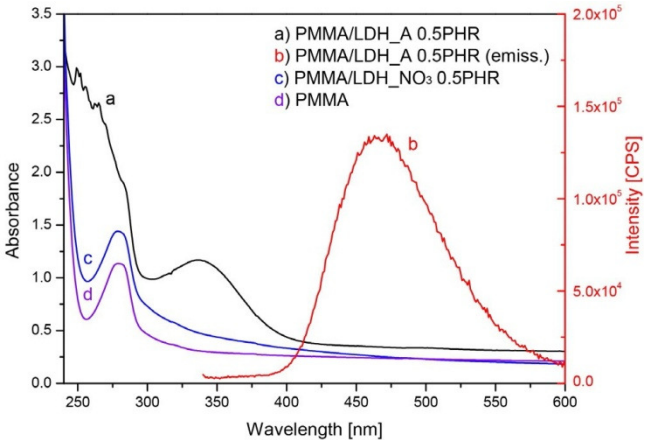

Figure 10. UV/Vis spectra of polymer films of a) PMMA compounded with LDH_A, c) PMMA compounded with LDH_NO3, and d) PMMA alone. b) Fluo- rescence emission spectra of PMMA compounded with LDH_A.

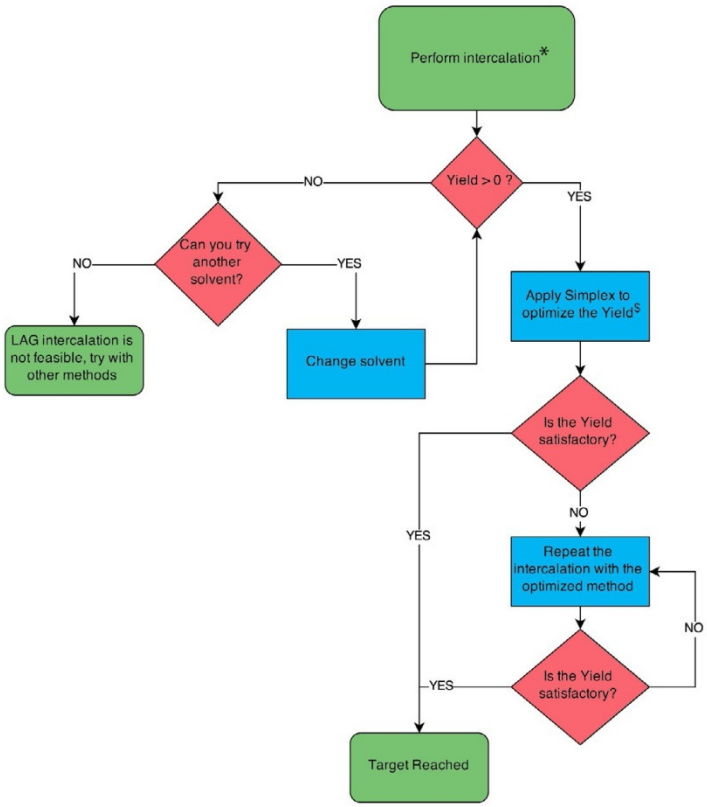

Figure 11. Flowchart for the testing and optimization of LAG intercalation of new guest molecules. *details in Ref. [29] $details in Ref. [30].